Observation of Landau levels and excitons at room temperature in $In_{0.53}Ga_{0.47}As/InP$ quantum wells

O. Jaschinski, M. Vergöhl, and J. Schoenes
Institut für Halbleiterphysik und Optik und Hochmagnetfeldanlage, Technische Universität Braunschweig, Mendelssohnstrasse 3, D-38106 Braunschweig, Germany

A. Schlachetzki and P. Bönsch
Institut für Halbleitertechnik, Technische Universität Braunschweig, Hans-Sommer-Strasse 66, D-38106 Braunschweig, Germany

(Received 5 May 1997)

We report on magneto-optical Kerr-ellipticity measurements with different $In_{0.53}Ga_{0.47}As/InP$ multi-quantum-wells at room temperature. These samples are grown with nominally the same sample parameters, except for the barrier thickness, which for one sample is small enough for a coupling between the quantum wells. The spectral range covered the quantum-well interband transitions of the electron–heavy-hole ground states. The magneto-optical spectra show a number of oscillations, whose spectral position depends on the magnetic-field strength. For model calculations, Lorentzian line shapes for the off-diagonal element of the dielectric tensor have been used. Magneto-optical interference effects are carefully discussed. For small magnetic fields, the shift of the ground state shows a diamagnetic behavior. For the coupled quantum well a transition into the high-field regime can be seen at $B \approx 9$ T. Due to the higher exciton energy for the uncoupled system, high-field behavior occurs only at fields beyond the range of the present experiments. Model calculations allow us to estimate from the shift of the ground state ($1s$), the exciton binding energy and the dimensionality of the system. According to these calculations the uncoupled sample shows a more 2D-like (where 2D is two-dimensional) behavior, while the coupled system is more 3D like. The higher levels, however, are typical for Landau splitting. For these the excitonic effect is negligible compared to the Landau shift. In our experiments, we were able to trace the oscillations up to 200 meV above the band gap of unstrained $In_{0.53}Ga_{0.47}As$ bulk material. This allows us to determine the energy dependence of the reduced effective mass at room temperature. Using the three-band Kane model for the calculation of the electron effective mass, we find that the hole effective mass in $In_{0.53}Ga_{0.47}As$ quantum wells is significantly lower than in bulk material. [S0163-1829(98)00919-9]

I. INTRODUCTION

Artificial two-dimensional (2D) electron systems, represented by semiconductor quantum-well structures, are of particular interest for the study of basic physical properties of semiconductors and find their application in a wide range of semiconductor devices. Due to the finite depth of the confinement potentials in real systems, it is impossible to fabricate perfect 2D systems. Therefore, the true dimensionality of systems with confinement in one direction is between two and three dimensions.[1] The examination of excitons in high magnetic fields (magnetoexcitons) is an excellent tool to study the dimensionality of a quantum-well structure, as was demonstrated by Hou *et al.*[2] and subsequently by Oettinger *et al.*[3] The diamagnetic shift of the magnetoexciton allows the determination of the extension of the exciton wave function in the well plane, which depends on the dimensionality of the system. Besides the effect on the excitonic state, the magnetic field also induces a Landau splitting of the valence- and conduction-band energy states. The coexistence of exciton diamagnetic shift and Landau levels was predicted theoretically by Akimoto and Hasegawa.[4] Several authors investigated the system $GaAs/Ga_xAl_{1-x}As$ theoretically[5,6] and experimentally,[7] concentrating on the excitonic ground state. The combination of exciton states and Landau levels was treated in[7–9] $GaAs/Ga_xAl_{1-x}As$ as well as in $Ga_xIn_{1-x}Sb/GaSb$.[10] In the latter case mechanical strain is present. This is also true when $In_xGa_{1-x}As$ is grown on GaAs substrates, so that the band parameters have to be modified. Such $In_xGa_{1-x}As$ quantum wells have been studied both experimentally[11] and theoretically.[12] Relatively few results have been reported on $In_{0.53}Ga_{0.47}As$ films on InP substrates[13–16] which can be considered as free of strain and where again the emphasis is on excitonic states.

Thus, there is a need to study $In_{0.53}Ga_{0.47}As$ quantum wells deposited lattice matched to InP, in particular, if the results do not apply only to low temperatures as in the references quoted above. In this paper we report on measurements of the magneto-optical Kerr ellipticity in $In_{0.53}Ga_{0.47}As/InP$ multi-quantum-wells at room temperature. Samples with different InP barrier widths were investigated. From the diamagnetic shift of the ground state of the electron–heavy-hole exciton (e-hh), the dimensionality of the electron system can be evaluated. The value of the exciton binding energy of coupled MQW's indicates the influence of the coupling on the carrier confinement. This effect has not yet been considered in the presently available theories. We present here the first experimental results. The energy dependence of the reduced effective mass, calculated

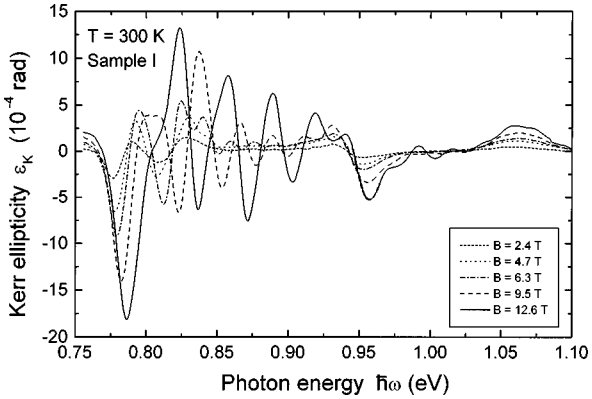

FIG. 1. Magneto-optical Kerr spectra of an $In_{0.53}Ga_{0.47}As/InP$ quantum well (sample I) at selected values of the magnetic induction B.

from the Landau shift, reflects the nonparabolicity of the band structure. We used Kane's three-band model[17] to evaluate our experiments. In addition, the results also reflect the effect of the confinement on the heavy-hole effective mass whose bulk value has to be modified.

II. EXPERIMENT

We have investigated two different, nominally undoped samples. They were grown by conventional metal-organic vapor-phase epitaxy in the low-pressure mode.[18] After depositing an InP buffer layer on top of the semi-insulating InP substrate the $In_{0.53}Ga_{0.47}As/InP$ MQW's were grown. The well thickness L_W was nominally 8 nm for both samples, whereas the nominal barrier thickness L_B was 10 nm for sample I and 6.6 nm for sample II. The layer sequence of 20 periods was capped by an InP film of 50 nm thickness. As determined by x-ray diffraction analysis, the lattice mismatch is lower than 0.02%.

The magneto-optical experiments have been done at 300 K in a standard Kerr spectrometer. We employed the sensitive 100%-polarization-modulation technique in which the magnetic circular dichroism can be traced down to 10^{-6} rad. The measurements have been performed in the spectral range between 0.7 and 1.1 eV in magnetic fields up to 15.2 T. Figures 1 and 2 show typical spectra of the magneto-optical

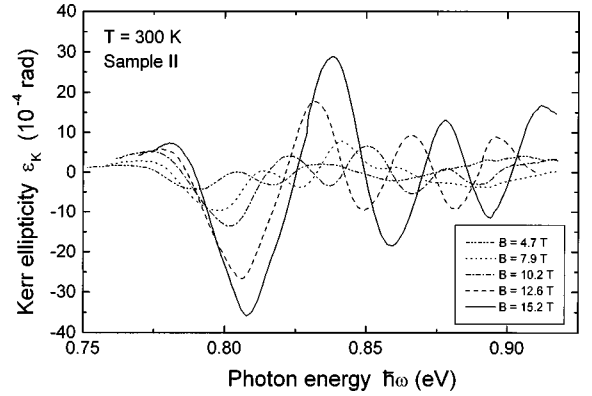

FIG. 2. Magneto-optical Kerr spectra of an $In_{0.53}Ga_{0.47}As/InP$ quantum well (sample II) at selected values of the magnetic induction B.

Kerr ellipticity of sample I and sample II, respectively. For clarity, only curves for selected values of the magnetic fields are displayed.

III. THEORY

A. Simulation of magneto-optical spectra

It is well known that interference effects in modulation spectroscopy of microstructures (photoreflectance,[19,20] electroreflectance[21]) may significantly alter the line shapes of the modulated spectra, even fake new interband transitions. In order to study the influence of these effects in the magneto-optical spectra of the quantum-well multilayers, we employed a matrix formalism described elsewhere.[22] This matrix calculus includes coherent optical and magneto-optical interference effects in thin multilayers. In the following, we will briefly describe the magneto-optical matrix theory. The complex magneto-optical Kerr effect (i.e., Kerr rotation Θ_K and Kerr ellipticity ε_K) of a multilayer system containing N plane-parallel homogeneous layers is given by the coefficients $\tilde{m}_{11}^{\pm}$ und $\tilde{m}_{12}^{\pm}$ of the resulting magneto-optical transfer matrix of the sample system:

$$\tilde{\Theta}_K = \Theta_K + i\ \mathrm{arctanh}(\varepsilon_K) = \frac{1}{2i} \times \ln\left(\frac{\tilde{m}_{11}^{+} \times \tilde{m}_{21}^{-}}{\tilde{m}_{11}^{-} \times \tilde{m}_{21}^{+}}\right) \qquad (1)$$

with

$$\begin{pmatrix} \tilde{m}_{11}^{\pm} & \tilde{m}_{12}^{\pm} \\ \tilde{m}_{21}^{\pm} & \tilde{m}_{22}^{\pm} \end{pmatrix} = \prod_{j=1}^{N} \begin{pmatrix} e^{+i\Phi_j^{\pm}} & 0 \\ 0 & e^{-i\Phi_j^{\pm}} \end{pmatrix} \times \frac{1}{\tilde{t}_{j,j+1}^{\pm}} \begin{pmatrix} 1 & \tilde{r}_{j,j+1}^{\pm} \\ \tilde{r}_{j,j+1}^{\pm} & 1 \end{pmatrix}.$$

and

$$\Phi_j^{\pm} = \frac{\omega}{c}\tilde{n}_j^{\pm}, \quad \tilde{r}_{j,j+1}^{\pm} = \frac{\tilde{n}_j^{\pm} - \tilde{n}_{j-1}^{\pm}}{\tilde{n}_j^{\pm} + \tilde{n}_{j+1}^{\pm}}, \quad \tilde{t}_{j,j+1}^{\pm} = \frac{2\tilde{n}_j^{\pm}}{\tilde{n}_j^{\pm} + \tilde{n}_{j+1}^{\pm}}.$$

The indices $+$ and $-$ relate to the σ^+ and σ^- modes of the electromagnetic wave in a longitudinal magnetic field, respectively. The complex factors of reflexion and transmission at the interface $j, j+1$ ($\tilde{r}_{j,j+1}^{\pm}$ and $\tilde{t}_{j,j+1}^{\pm}$, respectively) are functions of the complex magneto-optical refractive indices $\tilde{n}_j^{\pm}$ and $\tilde{n}_{j+1}^{\pm}$. The field-free optical constants of InP and $In_{0.53}Ga_{0.47}As$ required for the model calculations were taken from optical (reflexion and transmission) measurements.[23] For the 100%-polarization-modulation technique, switching the polarization directly between the two eigenmodes, the magneto-optical dielectric function $\tilde{\epsilon}^{\pm}$ can be written as:[24]

$$\tilde{\epsilon}^{\pm}(E,B) = \tilde{\epsilon}(E,B=0) \pm \Delta\tilde{\epsilon}(E,B) = \sum_{l=1}^{M} \left(\tilde{\epsilon}_l(E) \pm \tfrac{1}{2}\bar{g}_l \mu_B B \times \frac{\partial\tilde{\epsilon}_l(E)}{\partial E}\right) \qquad (2)$$

with l running over the critical points involved. $\bar{g}$ is the sum-g factor; μ_B is the Bohr magneton.

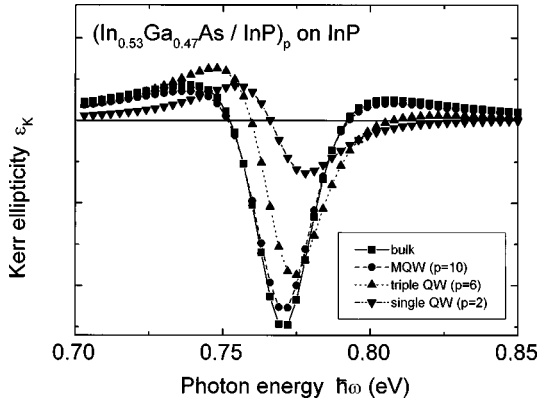

FIG. 3. Model calculations of the Kerr ellipticity using a Lorentzian line shape [Eq. (3)] for different numbers p of multilayer periods.

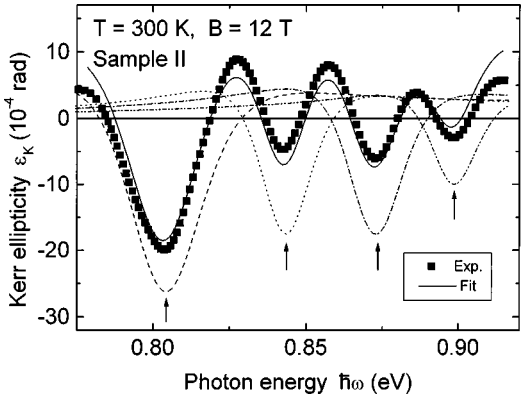

FIG. 4. Line-shape analysis of the Kerr spectra of sample II at $B=12$ T. Four Lorentzian oscillators are used. The energies corresponding to transitions are marked by arrows.

To describe the dispersion of localized excitons, Lorentzian line shapes

$$\tilde{\epsilon}_l(\hbar\omega,E_G,\Gamma,F)=\frac{F_l}{\hbar\omega-E_{G,l}+i\Gamma_l} \tag{3}$$

have been used. Here, $\hbar\omega$ is the photon energy, E_G is the gap energy, Γ is a broadening parameter, and F is the amplitude of the Lorentz oscillator.

If the refractive index n is much larger than the extinction coefficient k, the Kerr ellipticity is proprotional to the modulation Δn of n, so that, for a Lorentz oscillator, the maximum of ε_K determines the gap energy. However, in a multilayer system, this may no longer be true due to interference effects. In Fig. 3, a model calculation using Eq. (1) is shown for an $In_{0.53}Ga_{0.47}As/InP$ quantum well with different numbers p of periods. For the calculation of the magneto-optical Kerr ellipticity, a single Lorentzian [Eq. (3)] is assumed with $E_G=0.77$ eV and $\Gamma=20$ meV. The well and barrier thicknesses were both chosen as 6.6 nm, and the cap layer thickness as 50 nm. We observe a considerable shift of the extrema if p increases from 2 (down triangles) through 6 (up triangles) to 10 (dots). Between $p=10$ and the bulk material (squares) the shift is unresolvable. Thus, we conclude that for $p=20$, as in the present case, there is a negligible error as compared to the bulk material.

As an example Fig. 4 displays measurements (squares) taken with sample II at a magnetic field of 12 T in order to demonstrate our fitting procedure. Again we use Lorentzians to model the experimental results. We find four different resonances at the critical points (CP's) marked by arrows. The related resonance curves are shown as broken lines. Since ε_K contains absorptive as well as dispersive components, in general we cannot simply superimpose discrete resonances in ε_K. Instead the summation has to be done separately for the real and the imaginary part of the off-diagonal element of the dielectric tensor. This superimposition is shown as the solid line in Fig. 4. However, it should be mentioned that for $n \gg k$, as in the present case, the absorptive part of ε_K may be neglected and the result of the exact calculation does not differ substantially from the superposition of the discrete ε_K resonances.

We note that the lifetime broadening of the resonances is around 20 meV, i.e. close to k_BT at room temperature (k_B Boltzmann's constant, T absolute temperature). Although the CP's can be detected with an accuracy of less than 1 meV (depending on the mechanical reproducability of the spectrometer and its spectral resolution), the relatively large linewidth reduces the resolution if more than one CP is located within an energy interval of k_BT. This is the case at lower magnetic fields, where several CP's merge in the magneto-optical spectrum. This may lead to a wrong indentification of the quantum number.

In principle, each of the oscillators found by the fitting procedure consists of a doublet of the two Zeeman-split components. However, even assuming for the sum-g factor ($\bar{g}=g_c+g_v$) a value of ($\bar{g}\approx 10$),[25] the resulting spin splitting $\bar{g}\mu_B B$ is only 5 meV at $B=10$ T, which is too low to be observed at room temperature. On the other hand, this simplifies the model calculation because

$$\Delta\tilde{\epsilon}=\tilde{\epsilon}^+-\tilde{\epsilon}^-\approx\frac{\partial\tilde{\epsilon}(\hbar\omega)}{\partial\hbar\omega}\times\bar{g}\mu_B B \tag{4}$$

holds as already assumed in Eq. (2).

In some cases, an additional phase factor $\exp(i\Phi)$ is introduced in Eq. (3), describing the modification of the dispersion due to electron-hole interaction. Furthermore, the phase factor may be modified by Fano resonance, which is caused by the interaction of localized excitons with continuum states. We find that the simulation is negligibly improved by the introduction of a phase factor Φ as an additional fitting parameter, so that we do not consider it further.

The Seraphin coefficients, i.e., the optical constants used for the model calculations, were determined from $In_{0.53}Ga_{0.47}As$ homogeneous films and may differ from the values for the quantum wells. This may result in changes of the amplitudes, but not of the energies of the CP's. An error in these energies due to an error in the optical constants can be neglected given our spectral resolution, for two reasons: First, in our experimental conditions, the refractive index n is much larger than the extinction coefficient. Only n enters into the model equations, so that deviations in k, which indeed occur in quantum wells, can be neglected. Second, the change of n due to interband transitions in quantum wells is lower than 10%, as found by ellipsometry.[26] Therefore, the amplitudes of the calculated spectra will differ in that order

of magnitude, while the energy positions of the peaks are not affected. In summary, we have found that the simple Lorentzian line shapes can describe to a good approximation the magneto-optical dispersion of the $In_{0.53}Ga_{0.47}As/InP$ MQW samples.

B. Magnetoexcitons and Landau levels

In this subsection, we will describe the model that we have employed to explain the magnetic-field dependence of the energy levels in the quantum wells. In the following, it will be assumed that only dipole-allowed transitions occur, i.e., transitions between states with the same Landau quantum number m_L. Generally, the energy of an interband transition between the confined states in a magnetic field is given by

$$E = E_G + E_{\mathrm{hh}} + E_{\mathrm{e}} + E(B), \tag{5}$$

where E_G is the band gap of $In_{0.53}Ga_{0.47}As$ bulk material, E_{e} and E_{hh} are the confinement energies of electrons and holes, respectively. The last term $E(B)$ depends on the strength of the magnetic field. Two different cases have to be considered: the low-field case and the high-field case. Both will be discussed now.

The behavior of excitons in a magnetic field depends on the strength of the magnetic field. A theoretical description of hydrogenic excitons in magnetic fields of arbitrary strength is given by Akimoto and Hasegawa.[4] As shown in this work, one has to distinguish between the low-field range and the high-field range of the applied magnetic field. In the first case, in which the cyclotron energy of the electrons and holes is smaller than the binding energy of the corresponding exciton, the exciton shows a quadratic, diamagnetic energy shift with increasing magnetic field. From perturbation theory one obtains[14]

$$\Delta E_{\mathrm{dia}} = D_1 \frac{\epsilon_0^2 \epsilon_r^2 h^4 B^2}{4\pi^2 e^2 \mu^3}, \tag{6}$$

where e is the electron charge, h is Planck's constant, μ is the reduced effective mass, and $\epsilon_0 \epsilon_r$ is the permittivity of the host semiconductor. D_1 describes the dimensionality of the exciton system, taking values between 3/16 (2D) and 1 (3D). In the low-field case Eq. (5) becomes

$$E = E_G + E_{\mathrm{hh}} + E_{\mathrm{e}} + E_{\mathrm{ex}}(0) + \Delta E_{\mathrm{dia}}, \tag{7}$$

where $E_{\mathrm{ex}}(0)$ is the (negative) zero-field exciton binding energy. From Eq. (6) the dimensionality of the excitonic system can be obtained if the reduced effective mass is known.

In the case that the cyclotron energy of the electron-hole pair is greater than the binding energy of the exciton the cyclotron motion becomes dominant and leads to Landau levels for electrons and holes. These states are then subjected to electron-hole coupling. The binding energy of these states can be described by[8]

$$E_{\mathrm{ex}}(B) \approx 3\left(\frac{\hbar e B}{2(2m_L+1)\mu R_{\mathrm{ex}}}\right)^{1/2} R_{\mathrm{ex}} D_2, \tag{8}$$

where m_L denotes the quantum number of the Landau state, R_{ex} is the effective Rydberg constant of a 3D exciton, and

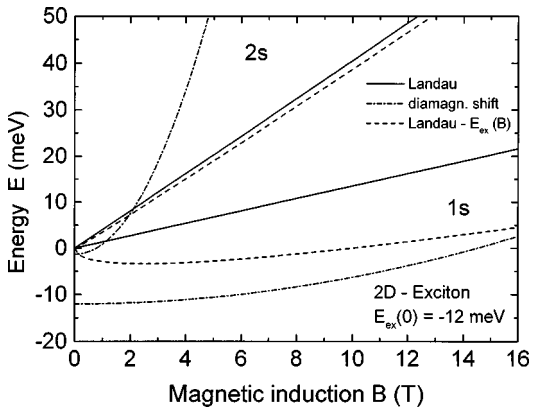

FIG. 5. Calculations of the Landau levels, the diamagnetic exciton shifts (low-field case) and the excitonic Landau levels (high-field case) for the ground state ($1s$) and the first excited state ($2s$) of a 2D exciton. Note that the excitonic states do not exist in the whole range of the plotted magnetic field.

D_2 a constant describing the dimensionality of the system ($D_2=1$ for 2D, $D_2=0.25$ for 3D). The total energy of an excitonic Landau state is the energy of the linear Landau state reduced by the binding energy $E_{\mathrm{ex}}(B)$. The transition energy [Eq. (5)] becomes

$$E = E_G + E_{\mathrm{hh}} + E_{\mathrm{e}} + E_{\mathrm{hh},m_L} + E_{\mathrm{e},m_L} + E_{\mathrm{ex}}(B), \tag{9}$$

where E_{hh,m_L} and E_{e,m_L} denote the mth Landau level of the heavy holes and electrons, respectively. The behavior of the $1s$ and $2s$ states of a 2D exciton [$E_{\mathrm{ex}}(0) = -12$ meV] in a magnetic field up to 16 T is displayed in Fig. 5. The diamagnetic energy shift (dash-dotted line) given by Eq. (7) is stronger than the increase of the energy level of an excitonic Landau level (dashed line) described by Eq. (9). This leads to a crossover of both curves at a distinct magnetic field (e.g., at ≈ 2 T for the $2s$ state). This crossing point marks the transition from the low-field to the high-field regime. The value of the magnetic field strength for this crossing point depends on the value of the exciton binding energy. For the ground state of the exciton as assumed in Fig. 5 the low-field case is valid in the whole range of the magnetic field displayed. For the $2s$ state, whose zero-field energy is smaller than for the $1s$ state, the transition between both field regimes occurs at a smaller magnetic field strength than for the $1s$ state. The energy of the excited exciton states can be calculated using the following expression:[1]

$$E_{\mathrm{ex},s,\alpha} = \frac{R_{\mathrm{ex}}}{[s+(\alpha-3)/2]^2}, \tag{10}$$

where s is the number of the state, and α is the dimensionality of the system. Due to the strong decrease of the zero-field energy of the excited states we do not expect unperturbed exciton states, whereas the ground state should exhibit a quadratic energy shift in the magnetic field range under consideration. For the high-field regime an excitonic nature of the energy states can be expected only for the ground state. As shown in Fig. 5 the difference between the excitonic Landau states and the true Landau states vanishes in case of the excited states. To summarize, we will expect an

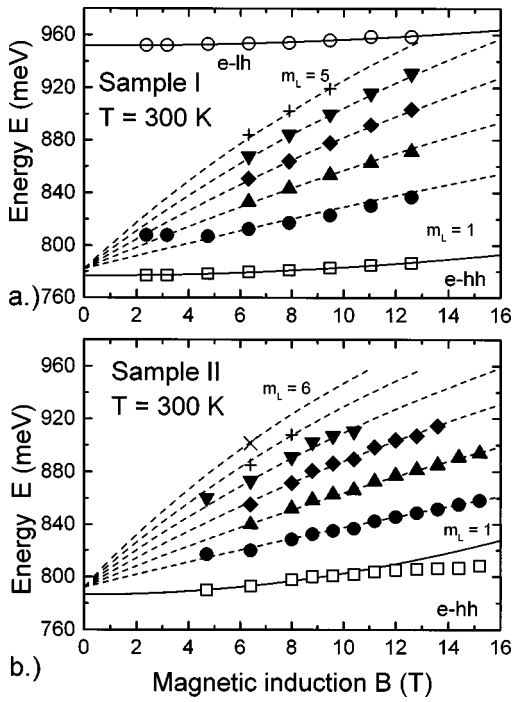

FIG. 6. Transition energies obtained from the line-shape analysis of sample I (a) and sample II (b), respectively. The excitonic transitions are marked by open symbols, the solid lines are quadratic fits. The Landau transitions are marked by full symbols. The Landau charts (dashed lines) are calculated taking into account the nonparabolicity of the conduction band.

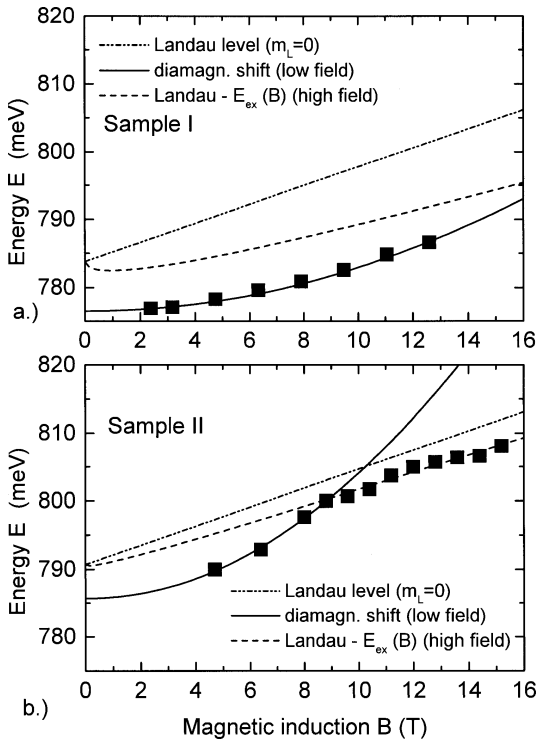

FIG. 7. (e-hh) ground states of both samples. The ground state of sample I (a) shows a clear diamagnetic shift in the whole magnetic field range, whereas the (e-hh)-exciton of sample II (b) exhibits a transition from the low-field to the high-field range around 9 T.

excitonic behavior of the ground state for both magnetic-field regimes and no resolvable excitonic magnetic-field dependence in case of the excited states. For these states we assume a true Landau shift.

IV. RESULTS AND DISCUSSION

A. Kerr spectra

The magneto-optical Kerr spectra of both samples reveal a number of distinct oscillations (Fig. 1 and Fig. 2). With increasing magnetic field the amplitude and the energy of the oscillations increase. Due to the thermal broadening, no spin splitting is observed. The experimental error in the Kerr ellipticity is less than 10^{-5} rad. The enhancement of the amplitude with higher fields originates from the increased modulation parameter of the polarization modulation. As discussed in the section on theory, the amplitude of the Kerr signal is proportional to the product of the joint spin splitting $(\overline{g}\mu_B B)$, and the amplitude of the critical points, i.e., the oscillator strength [cf. Eqs. (3) and (4)]. From Figs. 1 and 2, it can be seen that the increase of the amplitude of the lowest oscillation is superlinear, i.e., the oscillator strength increases with increasing magnetic field. This effect may originate from the shrinkage of the exciton wave function with increasing magnetic field, as found also by Zheng, Heiman, and Lax.[5] For the weakly coupled MQW, the shrinkage is more pronounced due to its more pronounced 3D character.

To obtain the energy states from the Kerr spectra we have carried out a line-shape analysis as described above, which showed that the minima of the oscillations correspond to the transition energies of the quantum well. The transition energies obtained from this analysis are plotted in Fig. 6(a) (sample I) and Fig. 6(b) (sample II). The solid lines are quadratic fits using Eq. (7). The dashed lines are true Landau states taking into account the nonparabolicity of the electron effective mass. Besides transition energies for the electron–heavy-hole exciton $E_{\text{e-hh}}$, we could determine the electron–light-hole exciton transition energy $E_{\text{e-lh}}$ (see Fig. 1). This peak is also blueshifted with field. At higher magnetic fields oscillations of transitions into excited states are visible.

B. Magnetoexcitons

As already discussed, we expect an excitonic behavior of the ground states. In verification we apply a fit based on Eq. (7). For sample I such a fit matches the data very well [Fig. 7(a), solid line]. This result proves that for the 1*s* state of the exciton of this sample the low-field approximation is valid up to at least 13 T. Using the value of μ as derived from the Landau transitions we obtain a dimensionality below 2 (the value of D_1 is smaller than 3/16). Therefore, it is neccessary to use an enhanced value of μ, which means that the exciton is a bound state. To estimate the zero-field binding energy $E_{\text{ex}}(0)$, which can be exactly calculated from the diamagnetic shift only in case of a perfect 2D or 3D system, we used the following procedure. Assuming a true 2D system, which may be reasonable for sample I, we obtain the reduced effective mass from Eqs. (6) and (7). This leads to the in-plane exciton radius r_{2D}, after[15]

$$\Delta E_{\text{dia}} = D_1 \frac{e^2 r_{\text{2D}}^2 B^2}{\mu}. \tag{11}$$

TABLE I. Values of the exciton parameters of sample I, determined from the diamagnetic shift.

r_{2D}	ρ	m_{hh}/m_0	m_e/m_0	μ/m_0	E_{ex}	R_{ex}
9 nm	11 nm	0.48	0.045	0.041	−7.3 meV	−2.9 meV

The relation between the radius r_{2D} of a 2D exciton and the extension ρ of its wave function is[27] $r_{2D}=\sqrt{3/2}\rho$ for a 2D system ($a_B=2r_{2D}$, a_B is the exciton Bohr radius). The value of ρ can be used to calculate the binding energy $E_{ex}(0)$ following the formalism described by Mathieu, Lefebvre, and Christol.[1] We find $E_{ex}(0)=-7.3$ meV. The values of the various parameters of the exciton are listed in Table I. The expected value of E_{ex} is -11.6 meV, which can be calculated from the binding energy R_{ex} of the corresponding 3D exciton using the relation $E_{ex}=4R_{ex}$, valid for an exact 2D system. The value of R_{ex} can be calculated using the value of μ, obtained from the diamagnetic shift. The difference between the expected and the measured value of E_{ex} demonstrates that sample I exhibits some deviations from the true 2D character. With the value of $R_{ex}=-2.9$ meV and a value of the heavy-hole effective mass $m_{hh}=0.48m_0$ we calculate the exciton shift in the high-field case [dashed line in Fig. 7(a)]. The transition between both field regimes should occur at around 18 T, which is out of the range of our equipment. Although these calculations are only an approximation it appears to be reasonable to conclude that the exciton system of sample I is close to the 2D case.

This is different for sample II [Fig. 7(b)]. The ground state shows a stronger energy shift as compared to sample I (e.g., $\Delta E\approx 10$ meV at 12.8 T for sample I, $\Delta E\approx 19$ meV at 12.8 T for sample II). This hints at a reduced exciton binding energy in sample II, which means that this sample is more 3D like than sample I. We estimate the binding energy and the dimensionality of the exciton. The procedure is similar to the previous case. We obtain the best fit to Eq. (7) if we use only the data measured in magnetic fields below 9 T. The diamagnetic shift is nearly three times larger than with sample I. This gives clear evidence of a decrease of the exciton binding energy. Unfortunately, it is impossible to estimate the binding energy from the diamagnetic shift because the dimensionality of the system is neither close to 2D nor to 3D. Thus assumptions are necessary. We assume that the reduced effective mass is the same as that of sample I. From the diamagnetic shift we find $D_1=0.53$. For magnetic fields above 9 T clear deviations from the quadratic fit occur. This might be caused by a transition from the low- to the high-field regime. To evaluate the dimensionality from the high-field measurements we rely on Eq. (9). The result is shown in Fig. 7(b) (dashed line). We find $D_2=0.35$. The binding energy can be determined from the difference of the fit for the low- and high-field range at $B=0$ T. For sample II we obtain $E_{ex}(0)=-5$ meV. All these results are indicative of the more 3D character of sample II. This can be explained by the two contributions of penetration of the exciton wave function into the barriers and of the overlap of the wave functions of adjacent quantum wells.[28] The enhancement of the coupling of the quantum wells of sample II is also confirmed by miniband calculations using the Kronig-Penney model. From these calculations we yield miniband widths of 0.5 meV for sample I and 4 meV for sample II.

C. Landau levels and effective masses

As shown above for the energy transitions to the excited states a nearly true Landau behavior is expected, but strong deviations from the linear energy shift are observed. This can be explained by the nonparabolicity of the conduction band. To describe the nonparabolicity the $\mathbf{k}\cdot\mathbf{p}$ theory by Kane[17] has been used. The total transition energy results from the band-gap energy of the well material, the confinement energies of the holes and electrons, calculated using the Kronig-Penney model, and the cyclotron energies of the holes and electrons. Assuming a parabolic valence band (or a constant heavy-hole effective mass m_{hh}) only the confinement energy and the cyclotron energy of the electrons are relevant for the energy dependence of the reduced effective mass μ. Using an iterative procedure for the energy dependence of the electron effective mass m_e, we are able to assign each transition energy to its corresponding Landau level [see Figs. 6(a) and 6(b)]. The values used in this procedure are given in Table II. Because of the excellent agreement between experiment and model calculation for up to six Landau levels it is posssible to determine the energy dependence of μ with high accuracy. The result is displayed in Fig. 8. As shown by several authors[29–34] the $\mathbf{k}\cdot\mathbf{p}$ theory represents an excellent description of the nonparabolicity of the conduction band, especially for $In_{0.53}Ga_{0.47}As$. Assuming a parabolic valence band we tried to fit our data with constant heavy-hole effective masses m_{hh} (solid and dashed curves in Fig. 8). The good quality of the fits corroborates the assumption leading to $m_{hh}=0.13m_0$ for sample I and to $m_{hh}=0.15m_0$ for sample II. These values are similar to the values found by Sugawara *et al.*[15] Both values are reduced compared to the value found in bulk $In_{0.53}Ga_{0.47}As$ (Ref. 35) demonstrating the influence of the dimensionality on the curvature of the valence band. The larger reduction occurs for sample I, which represents a more 2D-like system compared to sample II.

TABLE II. Values of parameters of $In_{0.53}Ga_{0.47}As$ used in the calculations described in the text.

m_e/m_0 [a]	m_{hh}/m_0 [b]	m_{lh}/m_0 [a]	ΔE_C [b]	ΔE_V [b]	Δ_0 [c]	E_G [b]	ϵ_r [b]
0.041	0.120	0.056	0.24 eV	0.37 eV	0.312 eV	0.74 eV	13.9

[a]Reference 36.
[b]Reference 15.
[c]Reference 37.

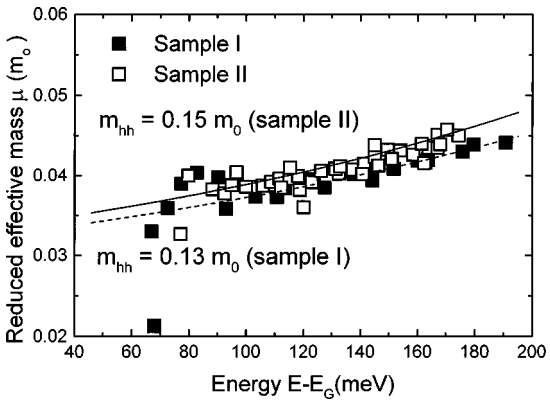

FIG. 8. Energy dependence of the reduced effective mass μ as derived from the Kerr spectra. The heavy-hole effective mass m_{hh} of sample I is significantly smaller than the bulk value demonstrating the influence of the dimensionality on the curvature of the valence band.

The difference between the energy of the crossing point of the Landau fan and the zero-field value of the exciton shift is commonly used as a measure of the binding energy of the exciton.[36,37] However, in the present case the values of the heavy-hole effective mass for the exciton ground state and the excited Landau states are different. Therefore, the difference between both states at zero field is no longer equal to the binding energy of the exciton.

V. CONCLUSIONS

In this paper we demonstrate the suitability of the magneto-optical Kerr effect to investigate excitonic and Landau states of MQW's at room temperature. Our measurements represent the first experimental proof of the coexistence of both kinds of states at room temperature. From the diamagnetic shift we estimate the dimensionality and the binding energy of the (e-hh) exciton. A comparison of two MQW's with identical well widths, but different barrier widths demonstrates the influence of the coupling of the exciton wave functions of adjacent quantum wells on the binding energy. In case of the more strongly coupled MQW, a transition from the low-field to the high-field regime is visible. This allows us to give a reasonable estimate of the binding energy in case of a dimension different from the true 2D or 3D case.

The excited states show no excitonic behavior. They can be explained by Landau shifts taking into account the nonparabolicity of the electron effective mass. The values of the heavy-hole effective mass, which we obtained from our measurements show the influence of the strength of the confinement on the curvature of the valence band.

ACKNOWLEDGMENTS

The authors wish to thank K. Dettmer and U. Thiele for the x-ray diffraction measurements. Two of the authors (M.V. and O.J.) are indebted to the Graduierten-Kolleg Metrologie in Physik und Technik (M.V.) and the German Science Foundation (O.J.), respectively, for financial support.

[1] H. Mathieu, P. Lefebvre, and P. Christol, J. Appl. Phys. **72**, 300 (1992).
[2] H. Q. Hou, W. Staguhn, S. Takeyama, N. Miura, Y. Segawa, Y. Aoyagi, and S. Namba, Phys. Rev. B **43**, 4152 (1992).
[3] K. Oettinger, Al. L. Efros, B. K. Meyer, C. Woelk, and H. Brugger, Phys. Rev. B **52**, R5531 (1995).
[4] O. Akimoto and H. Hasegawa, J. Phys. Soc. Jpn. **22**, 181 (1967).
[5] X. L. Zheng, D. Heiman, and B. Lax, Phys. Rev. B **40**, 10 523 (1989).
[6] R. L. Greene and K. K. Bajaj, Solid State Commun. **45**, 831 (1983).
[7] G. Duggan, Phys. Rev. B **37**, 2759 (1988).
[8] D. C. Rogers, J. Singleton, R. J. Nicholas, C. T. Foxon, and K. Woodbridge, Phys. Rev. B **34**, 4002 (1986).
[9] S. Tarucha, H. Okamoto, Y. Iwasa, and N. Miura, Solid State Commun. **52**, 815 (1984).
[10] R. J. Warburton, G. M. Sundaram, R. J. Nicholas, S. K. Haywood, G. J. Rees, N. J. Mason, and P. J. Walker, Surf. Sci. **228**, 270 (1990).
[11] D. C. Reynolds, D. C. Look, B. Jogai, and C. E. Stutz, Appl. Phys. Lett. **65**, 2293 (1994).
[12] K.S. Lee, Y. Aoyagi, and T. Sugano, Phys. Rev. B **46**, 10 269 (1992).
[13] J. Singleton, N. J. Pulsford, D. J. Mowbray, M. S. Skolnick, L. L. Taylor, S. J. Bass, R. J. Nicholas, and W. Hayes, J. Phys. Colloq. **48**, C5-147 (1987).
[14] D. J. Mowbray, J. Singleton, M. S. Skolnick, N. J. Pulsford, S. J. Bass, L. L. Taylor, R. J. Nicholas, and W. Hayes, Superlattices Microstruct. **3**, 471 (1987).
[15] M. Sugawara, N. Okazaki, T. Fujii, and S. Yamazaki, Phys. Rev. B **48**, 8848 (1993).
[16] M. Sugawara, Phys. Rev. B **45**, 11 423 (1992).
[17] E. O. Kane, J. Phys. Chem. Solids **1**, 249 (1957).
[18] E. Peiner, S. Mo, H. Iber, G.-P. Tang, and A. Schlachetzki, Thin Solid Films **283**, 226 (1996).
[19] N. Kallergi, B. Roughani, J. Aubel, S. Sundaram, J. Appl. Phys. **68**, 4656 (1990).
[20] O. J. Glembocki and B. V. Shanabrook, in *Semiconductors and Semimetals*, edited by R. K. Willardson and A. C. Beer (Academic, New York, 1993), Vol. 36, p. 221.
[21] A. C. Churchill, P. C. Klipstein, C. J. Gibbings, M. A. Gell, M. E. Jones, and C. G. Tuppen, Semicond. Sci. Technol. **6**, 18 (1991).
[22] R. Nies and F. R. Keßler, Phys. Status Solidi A **111**, 639 (1989).
[23] D. Hahn, O. Jaschinski, H.-H. Wehmann, A. Schlachetzki, and M. von Ortenberg, J. Electron. Mater. **24**, 1357 (1995).
[24] F. R. Keßler and J. Metzdorf, *Landau Level Spectroscopy: Interband Effects and Faraday Rotation* (Elsevier Publisher, Amsterdam, 1991).
[25] N. J. Traynor, R. T. Harley, and R. J. Warburton, Phys. Rev. B **51**, 7361 (1995).
[26] H. Iber, *Spektroskopische Ellipsometrie an III-V-Halbleiterstrukturen* (VDI-Verlag, Düsseldorf, 1996), Serie 8, No. 601.
[27] I. Aksenov, J. Kusano, Y. Aoyagi, T. Sugano, T. Yasuda, and Y.

Segawa, Phys. Rev. B **51**, 4278 (1995).
[28] P. Lefebvre, P. Christol, and H. Mathieu, Phys. Rev. B **46**, 13 603 (1992).
[29] M. Bugajski and W. Lewandowski, J. Appl. Phys. **57**, 521 (1985).
[30] D. Schneider, L. Elbrecht, J. Creutzburg, A. Schlachetzki, and G. Zwinge, J. Appl. Phys. **77**, 2828 (1995).
[31] D. Schneider, B. Tank, K. Beifuss, A. Schlachetzki, and D. Hahn, in *Proceedings of the Physical Phenomena at High Magnetic Fields-II*, edited by Z. Fisk *et al.* (World Scientific, Singapore, 1996), p. 104.
[32] C. Wetzel, Al. L. Efros, A. Moll, B. K. Meyer, P. Omling, and P. Sobkowicz, Phys. Rev. B **45**, 14 052 (1992).
[33] B. R. Nag and S. Mukhopadhyay, Appl. Phys. Lett. **62**, 2416 (1993).
[34] U. Wiesner, J. Pillath, W. Bauhofer, A. Kohl, A. Mesquida Küster, S. Brittner, and K. Heime, Appl. Phys. Lett. **64**, 2520 (1994).
[35] M. Sugawara, N. Okazaki, T. Fujii, and S. Yamazaki, Phys. Rev. B **48**, 8102 (1993).
[36] D. Gershoni, H. Temkin, and M. B. Panish, Phys. Rev. B **38**, 7870 (1988).
[37] E. H. Perea, E. E. Mendez, and C. G. Fonstad, Appl. Phys. Lett. **36**, 978 (1980).